

TOWARD FAITHFUL EXPLANATIONS IN ACOUSTIC ANOMALY DETECTION

Maab Elrashid^{1,2,3,4}, Anthony Deschênes^{3,4}, Cem Subakan^{1,2,4}, Mirco Ravanelli^{1,2}, Rémi Georges^{3,4}, Michael Morin^{3,4}

¹ Mila-Quebec AI Institute, QC, Canada, ² Concordia University, QC, Canada

³ FORAC Research Consortium, ⁴ Université Laval, QC, Canada

ABSTRACT

Interpretability is essential for user trust in real-world anomaly detection applications. However, deep learning models, despite their strong performance, often lack transparency. In this work, we study the interpretability of autoencoder-based models for audio anomaly detection, by comparing a standard autoencoder (AE) with a mask autoencoder (MAE) in terms of detection performance and interpretability. We applied several attribution methods, including error maps, saliency maps, SmoothGrad, Integrated Gradients, Grad-SHAP, and Grad-CAM. Although MAE shows a slightly lower detection, it consistently provides more faithful and temporally precise explanations, suggesting a better alignment with true anomalies. To assess the relevance of the regions highlighted by the explanation method, we propose a perturbation-based faithfulness metric that replaces them with their reconstructions to simulate normal input. Our findings, based on experiments in a real industrial scenario, highlight the importance of incorporating interpretability into anomaly detection pipelines and show that masked training improves explanation quality without compromising performance.

Index Terms— Explainable Artificial Intelligence, Audio Anomaly Detection, Faithfulness, Autoencoders.

1. INTRODUCTION

Anomaly detection plays a critical role in industrial monitoring, where early fault identification is essential [1]. For example, in wood manufacturing, equipment like planers relies on manual calibration, with limited real-time feedback on machine condition or product quality. Acoustic monitoring with low-cost microphones offers a promising alternative for anomaly detection, but remains challenging in noisy industrial environments where subtle acoustic cues can be easily masked [1, 2]. Recent deep learning approaches, particularly convolutional autoencoders with skip connections and transformer-based architectures, show superior performance in acoustic anomaly detection in this context [1]. However, their black-box nature limits trust in safety-critical environments, as models can exploit spurious features that correlate with anomalies but are not truly relevant [3, 4]. Interpretability avoids this by designing accurate models with correct explanations that enhance transparency and user trust [3].

In this work, we investigate the interpretability of anomaly detection using autoencoders on real industrial data from a wood planer [1]. We implement masked autoencoder (MAE) training [5] to improve feature learning. We apply several post-hoc explanation techniques, such as error maps and gradient-based methods [3], to analyze influential input regions. To validate the explanations, we match the anomaly intervals marked by experts and propose two metrics: an F-score for temporal overlap and a faithfulness score

to assess the impact of replacing highlighted regions on the model output¹.

In summary, our contributions include: (1) An interpretability study of gradient-based methods applied to autoencoders for acoustic anomaly detection; (2) adapting MAE-based training to improve anomaly localization; and (3) an evaluation protocol based on expert-annotated time segments and quantitative metrics that assess explanation relevance and faithfulness.

2. RELATED WORK

Autoencoders (AEs) are widely used for unsupervised anomaly detection (AD), due to their ability to learn compact representations and identify anomalies by reconstruction error [6, 7, 8]. However, AEs often struggle with precise anomaly localization. They can reconstruct anomalous instances, reducing error-based anomaly signals [9]. Additionally, they can react on irrelevant correlations, making interpretability important in critical applications [3].

To address these limitations, several works have applied post-hoc interpretability methods to AD using AEs, such as SHAP [10, 11], saliency maps, integrated gradients and SmoothGrad, which highlight input regions influence the anomaly score [3]. Yet, in unsupervised settings, such methods often lack clarity and robustness [12].

Beyond post-hoc methods, newer AE frameworks have been explored to inherently improve interpretability. Masked Autoencoders (MAEs) were originally proposed for self-supervised learning in vision, to learn semantically meaningful features by reconstructing masked inputs [5]. This strategy has been extended to AD in computer vision [13], medical imaging [14] and time series [15]. However, to the best of our knowledge, MAE-based methods, especially those tailored for spectrogram-based audio anomaly detection aimed at interpretability, have not yet been explored.

Furthermore, recent work emphasizes the importance of evaluating the explanation quality [3, 16]. Metrics such as the F-score assess plausibility against human-annotated anomalies [17], while Faithfulness measures how well the model explanations align with the model decision [18].

Our work builds on this foundation by applying MAE to industrial audio anomaly detection, with emphasis on interpretability rather than detection accuracy. We adapt the MAE framework to reconstruct masked spectrogram regions and derive explanations via error maps and gradient-based methods. Additionally, we introduce time-localized F-score and faithfulness metrics using expert annotations to quantify how well explanations align with human perception and model's decision making.

¹The annotated dataset and code are available at <https://github.com/MaabNimri/Faithful-Explanations-in-Acoustic-Anomaly-Detection>

Table 1: Dataset composition and anomaly types.

Training set (normal)		Test set (normal + anomalous)	
Count		3,235	
Anomaly types distribution (test set)			
Broken Board	Stuck Board	Uneven/Thick Board	
Count		4	29
			72

3. METHODOLOGY

3.1. Real Planing Mill Dataset

We use the publicly available dataset from [1], which comprises 7,562 mono 10-second recordings of an industrial wood planer, sampled at 20 kHz (~21 hours in total). Each audio clip is converted into an 80×401 mel spectrogram with a frame size of 50 ms, hop length of 25 ms, and 80 mel frequency bins.

The training set contains only normal recordings captured after maintenance and 10% of it is used for validation. The test set spans two days of planer operation and includes normal and anomalous samples (broken, stuck, and unevenly thick boards). Table 1 summarizes the data.

3.2. Anomaly Detection Models

3.2.1. Autoencoder

We adopt the Skip-CAE-Transformer from [1]; a reconstruction-based model that combines a convolutional autoencoder with skip connections and transformer blocks [19] for anomaly detection. The encoder extracts hierarchical representations from the input spectrogram using convolution, batch normalization, and pooling, followed by a transformer encoder. Skip connections are added and passed to the decoder, which mirrors the encoder structure and includes a transformer decoder for improved reconstruction.

The model is trained to minimize the Mean Squared Error (MSE) between the input and the reconstructed output.

3.2.2. Masked Autoencoder

Inspired by [5], we apply an adapted masked autoencoder (MAE) training strategy to our model. The model receives a randomly masked input X and learns to reconstruct only the masked regions, using the loss:

$$\mathcal{L}_{\text{MAE}} = \frac{1}{\sum_{i,j} M_{i,j}} \sum_{i,j} M_{i,j} (X_{i,j} - \hat{X}_{i,j})^2$$

where, M is the binary mask and \hat{X} is the reconstructed output.

This partial reconstruction objective forces the model to rely on contextual cues, which encourages meaningful feature learning.

We conducted an ablation study to select the mask ratio and patch size. Table 2 shows that 30% masking with 4×4 patches yields the best AUC (Area Under the ROC Curve), while extreme ratios or larger patches degrade performance [20]. Additionally, to ensure divisibility by patch size, the final time frame is removed, reducing the input to 400 frames with a negligible effect.

At inference, the model receives the full (unmasked) spectrogram and outputs a full reconstruction. Anomaly scores and attribution maps are computed using the mean squared error between input and output [14].

Table 2: AUC for MAE with varying mask ratios and patch sizes.

Mask Ratio (%)	AUC 4 \times 4 Patch Size	AUC 16 \times 16 Patch Size
90	0.842	0.808
75	0.864	0.710
50	0.842	0.710
30	0.902	0.636
15	0.821	0.569

Table 3: Anomaly types distribution in the annotated sample set.

	Broken Board	Stuck Board	Uneven/Thick Board
Count	2	10	34

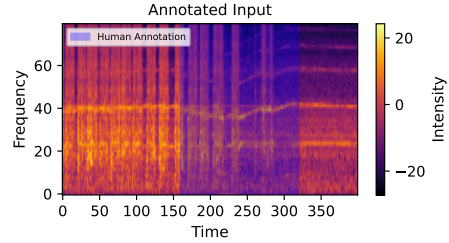


Fig. 1: Example of a human annotation for a broken board. The blue shaded region indicates the labeled anomaly interval.

3.3. Interpretability Methods

To analyze the model and localize anomalies, we apply several post-hoc interpretability methods using the Captum library². For gradient-based methods, we use the reconstruction mean squared error (MSE) as the scalar output for backpropagation [3], generating 2D attribution maps over the input spectrogram, highlighting the regions that contribute the most to the reconstruction error.

We apply pixel-wise error map [8], saliency-based techniques including Saliency Maps [21], Integrated Gradients [22], and SmoothGrad [23], as well as GradShap [24], which approximates SHAP values through gradient integration over randomized baselines. Furthermore, we use Grad-CAM [25] to highlight coarse regions by propagating gradients to the final convolutional layer of the encoder.

3.4. Interpretability Evaluation

3.4.1. Human Annotations

To assess the alignment between model explanations and human perception, 46 anomalous test recordings were annotated based on expert listening and spectrogram inspection, covering the 3 types of anomalies as in Table 3. Each annotation consists of one or more clearly audible anomalous intervals of at least one second (40 frames). Recordings with unclear acoustic signatures were excluded for quality. Figure 1 shows an example of annotation for a broken board.

²<https://captum.ai/>

3.4.2. Evaluation Metrics

We use two complementary metrics to evaluate explanation quality: the F-score and Faithfulness.

To compute the *F-score* [26], each 2D attribution map is collapsed into a 1D temporal signal by sum over frequency and normalization. Peaks are identified using high-percentile thresholding (e.g., 98th) and compared to the annotated 1-second intervals [27]. A true positive (TP) occurs if any peak falls within an annotated second. A false negative (FN) occurs when no peak is detected within an annotated second. A false positive (FP) is when a peak appears in an unannotated second [28].

Faithfulness evaluates whether regions highlighted by an attribution map meaningfully affect the reconstruction error [16]. We propose to estimate how the model would behave if the highlighted input region were instead “normal”.

Specifically, we replace the anomalous segments detected in the input X_1 with their reconstructed counterparts by the model \hat{X}_1 , resulting in a modified input X_2 and reconstruction \hat{X}_2 .

$$X_2 = M \cdot \hat{X}_1 + (1 - M) \cdot X_1$$

where, M is a binary mask over detected regions. We define the Faithfulness Score FF as:

$$FF = \max \left(1 - \frac{\text{Error}(\hat{X}_2, X_2)}{\text{Error}(\hat{X}_1, X_1)}, 0 \right)$$

Such that, if the replaced regions are irrelevant to the model’s decision, the reconstruction error changes little, resulting in a low FF score. Conversely, a higher FF means masking those regions significantly affects the error, indicating the explanation reliably highlights areas important to the model’s prediction.

We experimented with frame-based and segment-based replacement strategies. In *frame-based* (or *fidelity*), individual time frames containing detected peaks in the explanation map are replaced with their reconstructions [29], independent of human labels. In *segment-based*, entire 1-second segments are replaced if they contain at least one peak and overlap with human annotations to avoid dominating the reconstruction. This constrains the test to plausible anomaly regions, aligns with the concept of comprehensibility and human-aligned evaluation [16] [3], and complements the F-score.

Figure 2 shows a concrete example of segment-based replacement using the 1D MAE error map, where masking the identified regions effectively reduces the broken anomaly signal, and simulates a more normal pattern.

4. EXPERIMENTS AND RESULTS

We follow the same training setup as in [1], using AdamW [30] for 500 epochs with batch size 32. The learning rate starts at 10^{-3} , scheduled with a cosine annealing schedule [31], with a minimum of 10^{-5} and five warm-up cycles. Early stopping with patience of 30 epochs and model checkpointing based on validation loss are used. All experiments were run on a single 32GB GPU.

Anomaly Detection: The test AUC achieved by the standard autoencoder (AE) was 0.916, while the masked autoencoder (MAE) reached 0.902. However, due to the nondeterministic nature of the training, we repeated the experiments on five different random seeds. On average, AE achieved an AUC of 0.885 ± 0.032 , while MAE achieved 0.864 ± 0.048 . Despite this minor drop in detection performance, the MAE consistently produced more informative and localized attribution maps, as shown in interpretability evaluations.

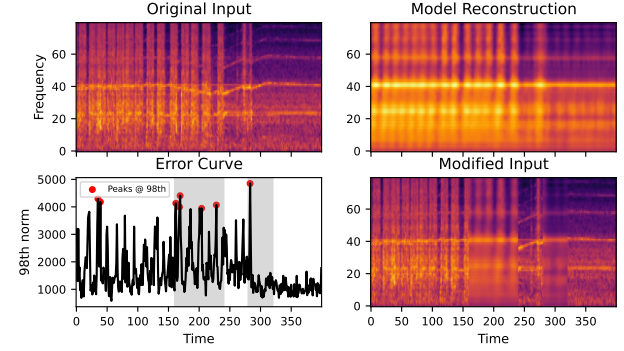


Fig. 2: Segment-based input replacement. Gray areas indicate regions selected by the MAE error map at the 98th percentile.

4.1. Interpretability Evaluation

4.1.1. F-score

We evaluated six interpretability methods across a range of high percentile thresholds (90th–99th) using F-score as a quantitative proxy for anomaly localization quality. As shown in Figure 4, the masked autoencoder (MAE) consistently outperforms the standard autoencoder (AE) across all methods. In particular, the highest score of 0.63 was achieved by MAE’s saliency map at the 98th percentile, compared to AE’s best of 0.55 from the error map at the 96th percentile.

4.1.2. Faithfulness

We evaluate the faithfulness of each method by measuring the drop in reconstruction error after replacing detected regions with the model’s reconstruction. From Figure 5, MAE-based explanations consistently yield higher faithfulness scores than AE-based ones across all methods and thresholds. The MAE Error Map, in particular, stands out as the most faithful explanation, at higher percentiles (95–98%), where it corresponds to the few most anomalous regions.

4.1.3. Qualitative Analysis

Figure 3 presents visual comparisons between attribution maps for a broken board anomaly. The MAE error map produces more localized and structured attribution map; that outlines the normal straight and abnormal non-straight horizontal lines within the annotated anomaly region, and more peaks are detected inside the annotated region, aligning well with human annotations. In contrast, the other attribution maps often produce scattered attributions or focus on irrelevant regions.

In summary, the results show that the MAE, despite a slightly lower detection AUC than the AE, produces better anomaly detection explanations. Among the MAE-based methods, the error map is the most reliable across both F-score and faithfulness evaluations. Saliency Map and SmoothGrad provide strong event localization, while Integrated Gradients and GradSHAP yield more faithful but less precise attributions. GradCAM performs the worst overall. This suggests the MAE’s potential for reliable explanations in real-world applications.

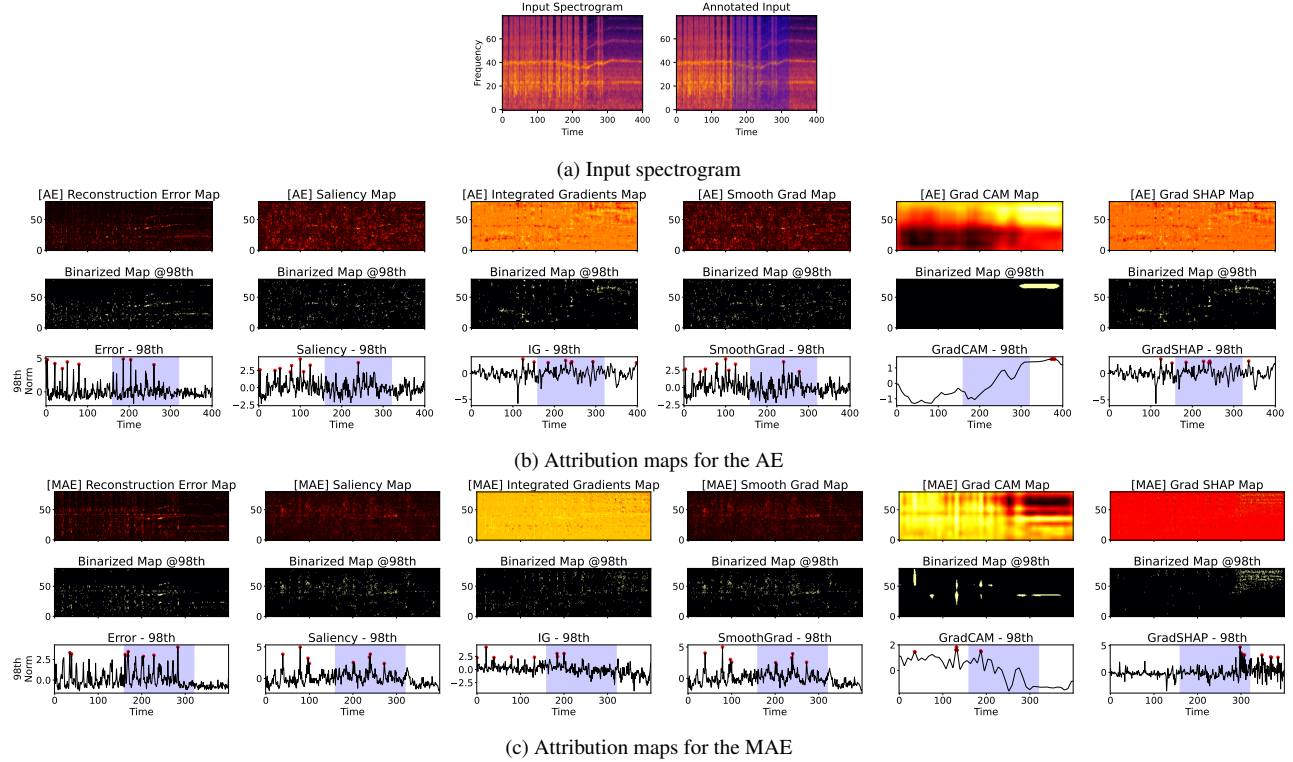


Fig. 3: Qualitative comparison of interpretability methods on a broken board anomaly. (a) shows the input spectrogram, with the input overlaid by human-annotated anomaly intervals. (b) and (c) display the raw 2D attribution maps from six methods, following their corresponding binarized masks at the 98th percentile, and the last row presents 1D temporal attribution signals collapsed over frequency at the 98th percentile, with red dots marking detected peaks and shaded regions indicating annotated anomalies, for the AE and MAE.

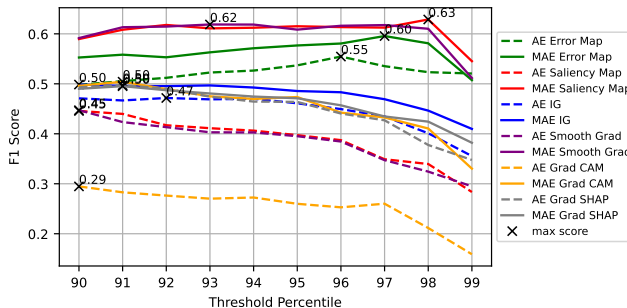


Fig. 4: F-score across different percentile thresholds (90th–99th) for all interpretability methods applied to AE and MAE models. The highest score for each method is marked with an “x”.

5. CONCLUSION

In this work, we investigated the interpretability of autoencoder-based acoustic anomaly detection using real industrial data, comparing a standard autoencoder (AE) and a masked autoencoder (MAE). We evaluated six post-hoc explanation methods using plausibility and faithfulness metrics. Although MAE achieved a slightly lower detection AUC than the AE model, it produced more temporally precise and faithful attribution maps, highlighting its strength in generating meaningful explanations. Among methods, MAE error maps

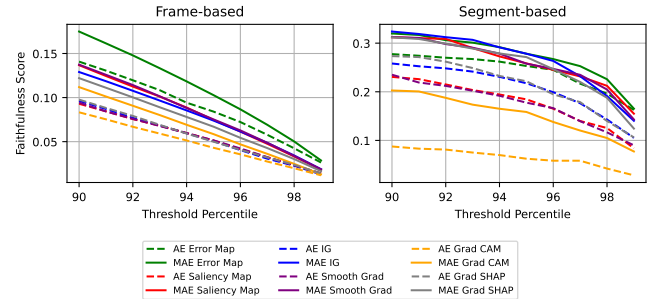


Fig. 5: Faithfulness scores across percentile thresholds (90th–99th).

offered consistent good detection precision, faithfulness, and structured attribution map. These findings suggest that MAE-based models improve interpretability with minimal impact on detection performance, making them suited for industrial applications where trust and actionable insights are essential.

6. REFERENCES

- [1] A. Deschênes, R. Georges, C. Subakan, B. Ugulino, A. Henry, and M. Morin, “Planing it by ear: Convolutional neural networks for acoustic anomaly detection in industrial wood planers,” in *Proc. of ICASSP*. IEEE, 2025, pp. 1–5.

[2] U. Buehlmann and R. E. Thomas, “Impact of human error on lumber yield in rough mills,” *Robotics and Computer-Integrated Manufacturing*, vol. 18, no. 3, pp. 197–203, 2002.

[3] Z. Li, Y. Zhu, and M. Van Leeuwen, “A survey on explainable anomaly detection,” *ACM Transactions on Knowledge Discovery from Data*, vol. 18, no. 1, pp. 1–54, 2023.

[4] S. Lapuschkin, S. Wäldchen, A. Binder, G. Montavon, W. Samek, and K.-R. Müller, “Unmasking clever hans predictors and assessing what machines really learn,” *Nature communications*, vol. 10, no. 1, pp. 1096, 2019.

[5] K. He, X. Chen, S. Xie, Y. Li, P. Dollár, and R. Girshick, “Masked autoencoders are scalable vision learners,” in *Proc. of CVPR*, 2022, pp. 16000–16009.

[6] Y. Koizumi, Y. Kawaguchi, K. Imoto, T. Nakamura, Y. Nikaido, R. Tanabe, H. Purohit, et al., “Description and discussion on dcase2020 challenge task2: Unsupervised anomalous sound detection for machine condition monitoring,” in *Workshop on Detection and Classification of Acoustic Scenes and Events*, 2020.

[7] E. Marchi, F. Vesperini, F. Eyben, S. Squartini, and B. Schuller, “A novel approach for automatic acoustic novelty detection using a denoising autoencoder with bidirectional lstm neural networks,” in *Proc. of ICASSP*. IEEE, 2015, pp. 1996–2000.

[8] D. Zimmerer, F. Isensee, J. Petersen, S. Kohl, and K. Maier-Hein, “Unsupervised anomaly localization using variational auto-encoders,” in *Proc. of MICCAI*. Springer, 2019, pp. 289–297.

[9] R. Bouman and T. Heskes, “Autoencoders for anomaly detection are unreliable,” *arXiv preprint arXiv:2501.13864*, 2025.

[10] K. Roshan and A. Zafar, “Utilizing xai technique to improve autoencoder based model for computer network anomaly detection with shapley additive explanation(shap),” *International Journal of Computer Networks & Communications*, 2021.

[11] L. Antwarg, R. M. Miller, B. Shapira, and L. Rokach, “Explaining anomalies detected by autoencoders using shap,” *arXiv preprint arXiv:1903.02407*, 2019.

[12] J. Tritscher, A. Krause, and A. Hotho, “Feature relevance xai in anomaly detection: Reviewing approaches and challenges,” *Frontiers in Artificial Intelligence*, vol. 6, pp. 1099521, 2023.

[13] Chaoqin Huang, Qinwei Xu, Yanfeng Wang, Yu Wang, and Ya Zhang, “Self-supervised masking for unsupervised anomaly detection and localization,” *IEEE transactions on multimedia*, 2022.

[14] M.-I. Georgescu, “Masked autoencoders for unsupervised anomaly detection in medical images,” *Procedia Computer Science*, vol. 225, pp. 969–978, 2023.

[15] D. Lee, S. Malacarne, and E. Aune, “Explainable time series anomaly detection using masked latent generative modeling,” *Pattern Recognition*, vol. 156, pp. 110826, 2024.

[16] C. S. Chan, H. Kong, and L. Guanqing, “A comparative study of faithfulness metrics for model interpretability methods,” in *Proc. of ACL*, 2022, pp. 5029–5038.

[17] S. Holly, R. Heel, D. Katic, L. Schoeffl, A. Stiftinger, P. Holzner, T. Kaufmann, et al., “Autoencoder based anomaly detection and explained fault localization in industrial cooling systems,” *PHM Society European Conference*, 2022.

[18] I. Šimić, Eduardo Veas, and V. Sabol, “A comprehensive analysis of perturbation methods in explainable ai feature attribution validation for neural time series classifiers,” *Scientific Reports*, vol. 15, no. 1, pp. 26607, 2025.

[19] A. Vaswani, N. Shazeer, N. Parmar, J. Uszkoreit, L. Jones, A. N Gomez, et al., “Attention is all you need,” *Advances in neural information processing systems*, vol. 30, 2017.

[20] L. Kong, M. Q Ma, G. Chen, E. P Xing, Y. Chi, L.-P. Morency, and K. Zhang, “Understanding masked autoencoders via hierarchical latent variable models,” in *Proc. of CVPR*, 2023, pp. 7918–7928.

[21] K. Simonyan, A. Vedaldi, and A. Zisserman, “Deep inside convolutional networks: Visualising image classification models and saliency maps,” *arXiv preprint arXiv:1312.6034*, 2013.

[22] M. Sundararajan, A. Taly, and Q. Yan, “Axiomatic attribution for deep networks,” in *Proc. of ICML*. PMLR, 2017, pp. 3319–3328.

[23] D. Smilkov, N. Thorat, B. Kim, F. Viégas, and M. Wattenberg, “Smoothgrad: removing noise by adding noise,” *arXiv preprint arXiv:1706.03825*, 2017.

[24] S. M Lundberg and S.-I. Lee, “A unified approach to interpreting model predictions,” *Advances in neural information processing systems*, vol. 30, 2017.

[25] R. R Selvaraju, M. Cogswell, A. Das, R. Vedantam, D. Parikh, and D. Batra, “Grad-cam: Visual explanations from deep networks via gradient-based localization,” in *Proceedings of ICCV*, 2017, pp. 618–626.

[26] D. M. W. Powers, “Evaluation: from precision, recall and f-measure to roc, informedness, markedness and correlation,” *arXiv preprint arXiv: 2010.16061*, 2020.

[27] O. Gungor, A. Rios, P. Mudgal, N. Ahuja, and T. Rosing, “A robust framework for evaluation of unsupervised time-series anomaly detection,” in *Proc. of ICPR*. Springer, 2024, pp. 48–64.

[28] M. El Amine Sehili and Z. Zhang, “Multivariate time series anomaly detection: Fancy algorithms and flawed evaluation methodology,” in *Proc. of Tech. Conf. on Perf. Eval. and Benchmarking*. Springer, 2023, pp. 1–17.

[29] T. T. Nguyen, T. Le Nguyen, and G. Ifrim, “Robust explainer recommendation for time series classification,” *Data Mining and Knowledge Discovery*, vol. 38, no. 6, pp. 3372–3413, 2024.

[30] I. Loshchilov and F. Hutter, “Decoupled weight decay regularization,” *arXiv preprint arXiv:1711.05101*, 2017.

[31] I. Loshchilov and F. Hutter, “SGDR: Stochastic gradient descent with warm restarts,” in *Proc. of ICLR*, 2017.